A Dorsolateral Prefrontal Cortex Semi-Automatic Segmenter

Ramsey Al-Hakim[a], James Fallon[b], Delphine Nain[c], John Melonakos[d], Allen Tannenbaum[d]

[a]Department of Biomedical Engineering, Georgia Institute of Technology, Atlanta GA 30332
[b]Department of Anatomy and Neurobiology, University of California, Irvine CA 92697
[c]College of Computing, Georgia Institute of Technology, Atlanta GA 30332
[d]Department of Electrical Engineering, Georgia Institute of Technology, Atlanta GA 30332

1. DESCRIPTION OF PURPOSE

Structural, functional, and clinical studies in schizophrenia have, for several decades, consistently implicated dysfunction of the prefrontal cortex in the etiology of the disease. Functional and structural imaging studies, combined with clinical, psychometric, and genetic analyses in schizophrenia have confirmed the key roles played by the prefrontal cortex and closely linked "prefrontal system" structures such as the striatum, amygdala, mediodorsal thalamus, substantia nigra-ventral tegmental area, and anterior cingulate cortices. The nodal structure of the prefrontal system circuit is the dorsal lateral prefrontal cortex (DLPFC), or Brodmann area 46, which also appears to be the most commonly studied and cited brain area with respect to schizophrenia.[1, 2, 3, 4] In 1986, Weinberger et. al. tied cerebral blood flow in the DLPFC to schizophrenia.[1] In 2001, Perlstein et. al. demonstrated that DLPFC activation is essential for working memory tasks commonly deficient in schizophrenia.[2] More recently, groups have linked morphological changes due to gene deletion and increased DLPFC glutamate concentration to schizophrenia.[3, 4]

Despite the experimental and clinical focus on the DLPFC in structural and functional imaging, the variability of the location of this area, differences in opinion on exactly what constitutes DLPFC, and inherent difficulties in segmenting this highly convoluted cortical region have contributed to a lack of widely used standards for manual or semi-automated segmentation programs.

Given these implications, we developed a semi-automatic tool to segment the DLPFC from brain MRI scans in a reproducible way to conduct further morphological and statistical studies. The segmenter is based on expert neuroanatomist rules (Fallon-Kindermann rules), inspired by cytoarchitectonic data and reconstructions presented by Rajkowska and Goldman-Rakic.[5] It is semi-automated to provide essential user interactivity. We present our results and provide details on our DLPFC open-source tool.

2. METHOD

In the present study, we have used cytoarchitectonic data and reconstructions presented by Rajkowska and Goldman-Rakic[5] to develop localization and segmentation rules for DLPFC for a semi-automated program.

2.1. Neuroanatomical Rules

The neuranatomical rules for determining the DLPFC are as follows:

1. In AC-PC space, determine the most anterior point of the brain (frontal pole) in the hemisphere you wish to draw. This must be done for each hemisphere separately and recorded in mm locations and distances (See Figure 1).

2. In AC-PC space, determine the point for the tip of the temporal pole in the hemisphere you wish to draw. This must be done for each hemisphere separately and recorded in mm locations and distances (See Figure 2).

Medical Imaging 2006: Image Processing, edited by Joseph M. Reinhardt, Josien P. W. Pluim,
Proc. of SPIE Vol. 6144, 61440J, (2006) · 0277-786X/06/$15 · doi: 10.1117/12.653643

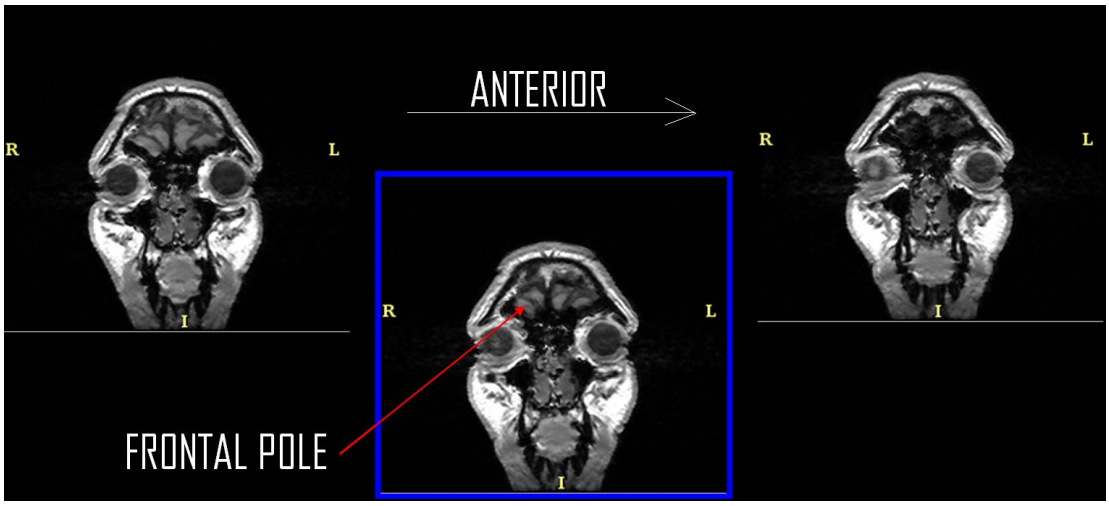

Figure 1. Step 1 of the neuroanatomical rules: Locating the Frontal Pole

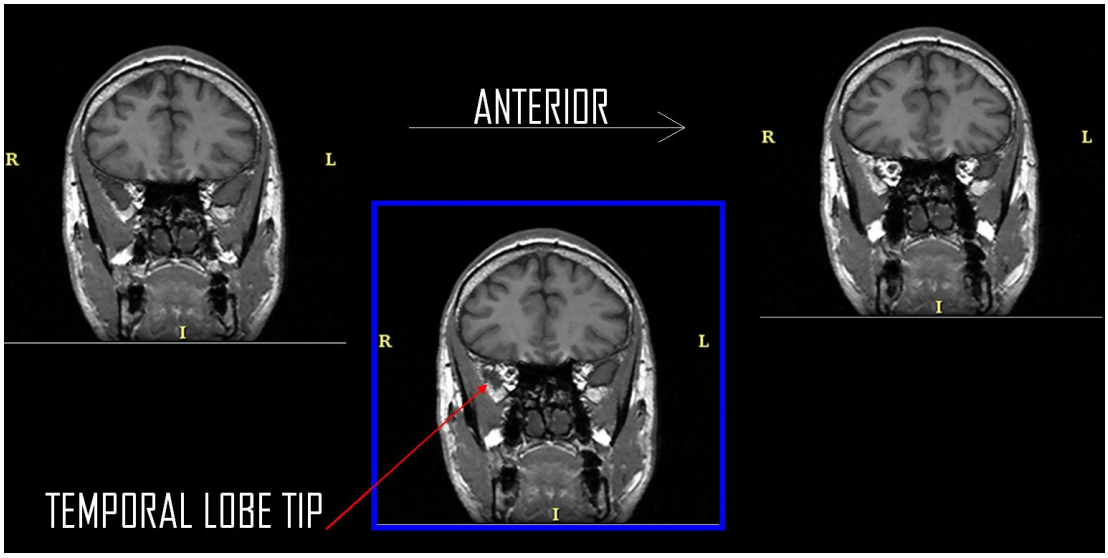

Figure 2. Step 2 of the neuroanatomical rules: Locating the Temporal Lobe Tip

3. The average distance (as a percent) from the tip of the temporal lobe to the posterior vertical boundary of the DLPFC parallelogram is 20% of $\sim$ 50 mm, or $\sim$ 10 mm; the average distance from the tip of the frontal pole and the anterior vertical boundary of the DLPFC parallelogram is 40% of $\sim$ 50 mm, or $\sim$ 20 mm. These proportionalities will be used to determine the posterior and anterior boundary of the DLPFC. Figure 3 shows these boundaries.

4. The DLPFC will never be above the inferior bank of the superior frontal sulcus nor below the superior bank of the inferior frontal sulcus. The deeper, more medial, portions ("tails") of the middle frontal sulcus may, however, lie inferior to the superior bank of the inferior frontal sulcus and should be included. These idealized sulci are shown in Figure 4.

5. The DLPFC is always above the 50% mark for the inferior-to-superior distance on a given coronal slice. It is not necessarily in the same relative position in both hemispheres.

Further author information: (Send correspondence to: Ramsey Al-Hakim: E-mail: ramsey@gatech.edu)

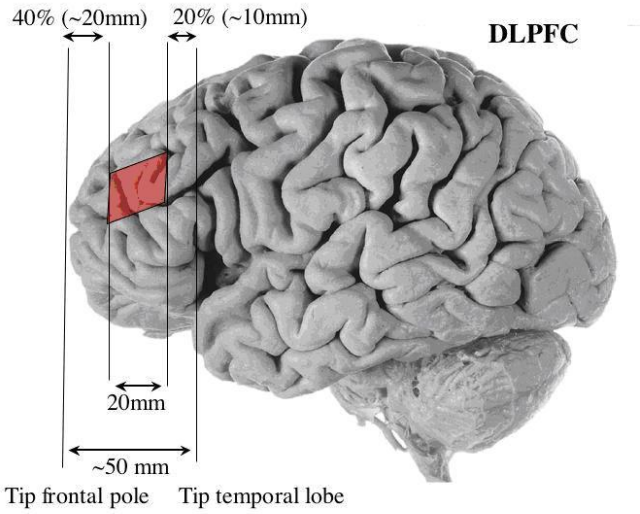

Figure 3. Boundary Rules to identify DLPFC (shaded area)

6. The superior border of the DLPFC will be (generally) 20 mm superior to the middle frontal sulcus. This means that your drawn boundary can change position toward the dorsal surface as you move posteriorly.

7. To locate and track the middle frontal gyrus as it moves and changes as it proceeds posteriorly, begin anterior to the anterior boundary, and watch where the boundaries of the gyrus moves as you proceed posteriorly through the slices to the temporal lobe tip. Move in the opposite direction beginning from posterior to the posterior boundary. Perform these steps separately and several times for each hemisphere. The information will help guide you as the boundaries change shape and position. The middle frontal gyrus is shown in Figure 4.

8. Include in the DLPFC:

   (a) The cortical ribbon from the midpoint deep in the lower bank of the superior frontal sulcus to the midpoint deep in the upper bank of the inferior frontal sulcus. This means that you will outline against cerebral spinal fluid on the outer surface as well as against white matter on the inner surface. Lighter gray (not white) voxels should be included.

   (b) Any gray matter lying medially to this ribbon that is part of the middle frontal gyrus within the anterior-posterior boundaries as outlined above.

9. Exclude obvious white matter voxels unless the mask voxel includes gray and white matter. This is because Layer VIB of the cortical ribbon, which contains few cell bodies and thus is not as gray as the other layers at the gray-white junction, would be excluded if the mask covered only dark gray voxels.

10. When areas of middle frontal gyrus are below the 50% mark, begin the trace at the surface superior to the 50% mark only, even though it appears that the upper bank of the inferior frontal gyrus will be excluded.

11. Check the surface ("as the crow flies") distance between the superior and inferior boundaries of the mask on a coronal slice by noting the coordinates of its superior and inferior boundaries. Superimpose a virtual right triangle, calculate the distance for each leg, then compute the hypotenuse value. This value should be approximately 20 + 2 mm.

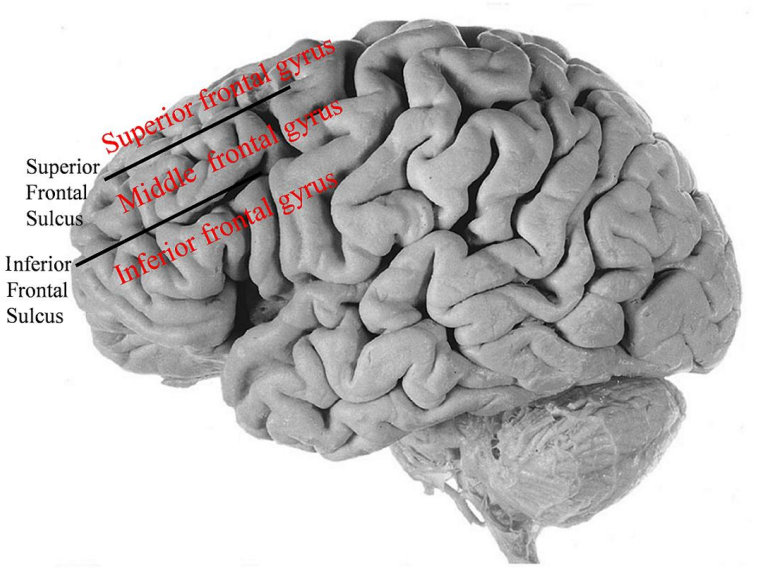

Figure 4. Idealized sulci and gyri pertinent to locating the DLPFC

2.2. Semi-Automatic Algorithm

For the semi-automatic segmentation, a brain MRI scan is shown coronally to the user in a display window. The user can scroll through the slices manually and click with the mouse to identify landmarks requested by the algorithm. The user's first step is to locate the temporal lobe tip and frontal pole (rules 1 and 2). The anterior and posterior boundaries are subsequently calculated automatically based on fixed proportional distances from these landmarks based on rule 3 (See Figure 3). With a few clicks, the user defines the remaining boundaries following the sulci based on the remaining neuroanatomical rules 4-11 to create a region of interest (ROI) that includes gray matter specific to the DLPFC. Neighboring cerebral spinal fluid (CSF) and white matter that surround the DLPFC may also be included in the ROI. A sample of the ROI that is required is shown in Figure 5.

Within the ROI, we are only interested in the gray matter segment, which corresponds to the DLPFC. In order to separate white matter, gray matter, and cerebral spinal fluid (CSF), we apply a Bayesian segmentation.[6] The Bayesian segmentation takes as an input the raw data from the ROI and produces a label map of the three classes: gray matter, white matter, and CSF.

We assume that the value of each voxel intensity in a given class can be considered as a random variable, independent across pixels. Furthermore, we assume that the voxel intensities are normally distributed. With a large set of training data, the distributions may also be learned a priori. In these results, we use k-means clustering to estimate the means and variances for the distribution of each class.

The application of the statistical distributions to the voxel intensities produces the membership probabilities, $Pr(Vi = v|Ci = c)$. The prior probabilities, $Pr(Ci = c)$, of a pixel belonging to a particular class are assumed to be uniform.

Using the membership and prior probabilities, we generate the posterior probabilities via Bayes' Rule. Finally, using the maximum a posteriori (MAP) estimate on the posterior probabilities, the final labelmap is produced.

Teo et. al. and Haker et. al. have shown that smoothing the posteriors prior to applying the MAP estimate can often yield improved segmentations.[7, 8, 9] Accordingly, we smooth for several iterations to remove noise and yield smooth segmentations.

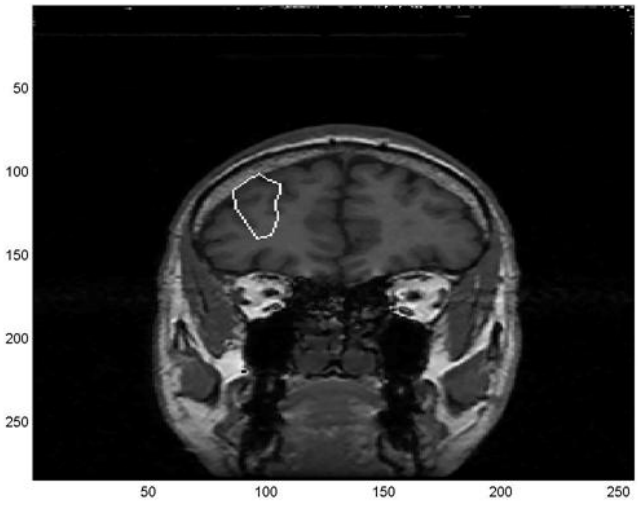

Figure 5. A sample of the ROI that is needed for the semi-automatic algorithm

The model is then visualized in 3D Slicer (freely available at `http://www.slicer.org`). The full semi-automatic algorithm is in the process of being included in the NA-MIC toolkit (`http://www.na-mic.org`) and will be available as a free open-source module of 3D Slicer by the end of 2006.

3. RESULTS

In this section, we compare the results of the semi-automatic segmenter against two expert manual segmentations of 10 brain datasets (5 different brain sets were used for each expert). The 5 patients' heads were imaged in the coronal plane with a 1.5 T MRI system* with a postcontrast 3D sagittal spoiled gradient recalled (SPGR) acquisition with contiguous slices. The resolution is $0.975 \times 0.975 \times 1.5$ mm ($256 \times 256 \times 123$ voxels). The expert manual segmentations were obtained by using the editor module of 3D Slicer in an average of 45 minutes per case. The semi-automatic segmentations were obtained with our software, in an average of 5 minutes per case. To validate the results of the semi-automatic segmenter, for each case we randomly picked 3 coronal slices that intersect the DLPFC structure and for each slice compared the semi-automatic segmentation (S) to the ground truth manual segmentation (G) using the DICE coefficient[10]: $DSC(S,G) := \frac{V_{S \cap G}}{\frac{1}{2}(V_S + V_G)}$, where V_X is the volume (number of voxels) of segmentation X.

	Case 1	**Case 2**	**Case 3**	**Case 4**	**Case 5**	**Mean**	**Std. Dev.**
Slices	[100,105,106]	[100,104,107]	[103,105,107]	[103,107,110]	[102,105,108]		
DSC(%)	0.8238	0.8035	0.7840	0.8178	0.7311	0.7920	0.0374

Table 1. Validation measure (DICE) for DLPFC segmentation by semi-automatic algorithm and expert 1 on real datasets.

	Case 6	**Case 7**	**Case 8**	**Case 9**	**Case 10**	**Mean**	**Std. Dev.**
Slices	[181,185,189]	[208,211,215]	[174,175,185]	[165,166,168,171]	[171,175,180]		
DSC(%)	0.6378	0.7795	0.7238	0.7281	0.7558	0.7250	0.0537

Table 2. Validation measure (DICE) for DLPFC segmentation by semi-automatic and expert 2 on real datasets.

*Signa, GE Medical Systems, Milwaukee, WI.

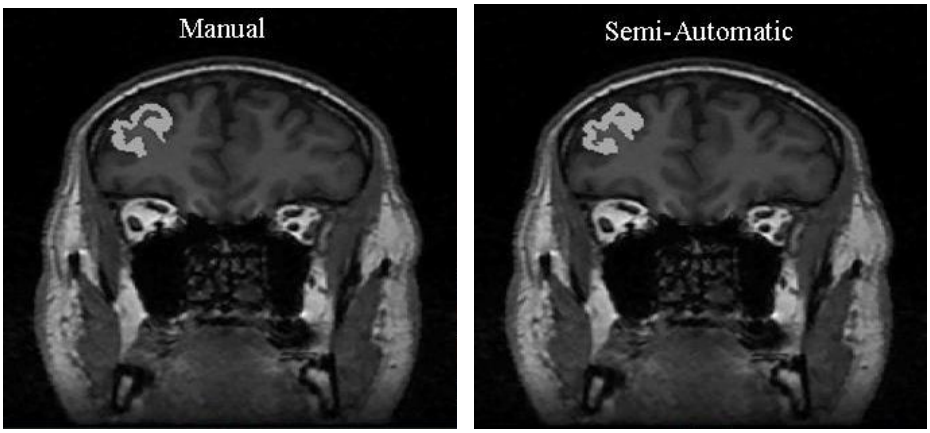

(a) Manual Segmentation (b) Semi-Automatic Segmentation

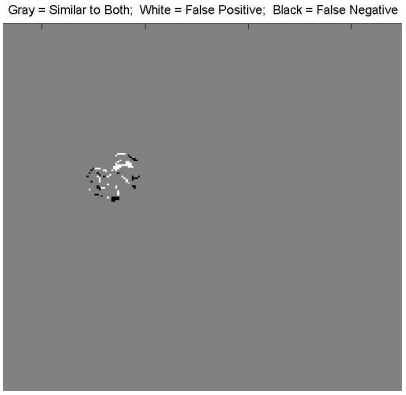

(c) Difference between Manual and Semi-Automatic Segmentation

Figure 6. Segmentation Results for Case 2, Slice 100

The results in Tables 1 and 2 show that the semi-automatic segmenter gives very good results. The Mean DSC coefficients for expert 1 is 0.7920 and the Mean DSC coefficient for expert 2 is 0.7250 (for $N = 5$ cases each). A DSC coefficient > 0.7 is regarded as good agreement in the literature.[10] Furthermore, there is a low variability across cases (Std. Dev. DSC expert 1=0.0374 and Std. Dev. DSC expert 2=0.0537 for $N = 5$ cases each). The result of a typical segmentation compared to the ground truth is shown in Figure 6(a),6(c) and the resulting 3D models are shown in Figure 7. A model of the left and right DLPFC are shown as viewed in 3D-SLICER in Figure 8.

4. CONCLUSION

We developed a semi-automatic segmenter to assist in the segmentation of the DLPFC from brain MRI scans. By including expert rules in the segmentation framework, we are able to segment the DLPFC semi-automatically and reduce the segmentation time from 45 minutes to 5 minutes with excellent segmentation results.

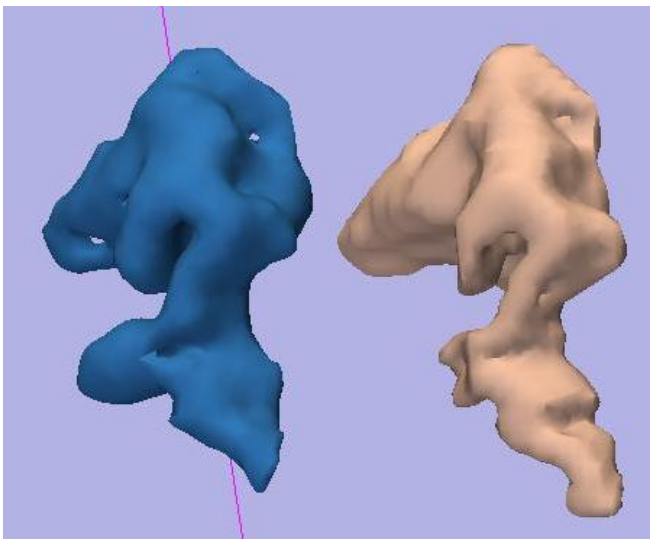

Figure 7. DLPFC 3D Models: Manual (Left), Semi-Automatic (Right)

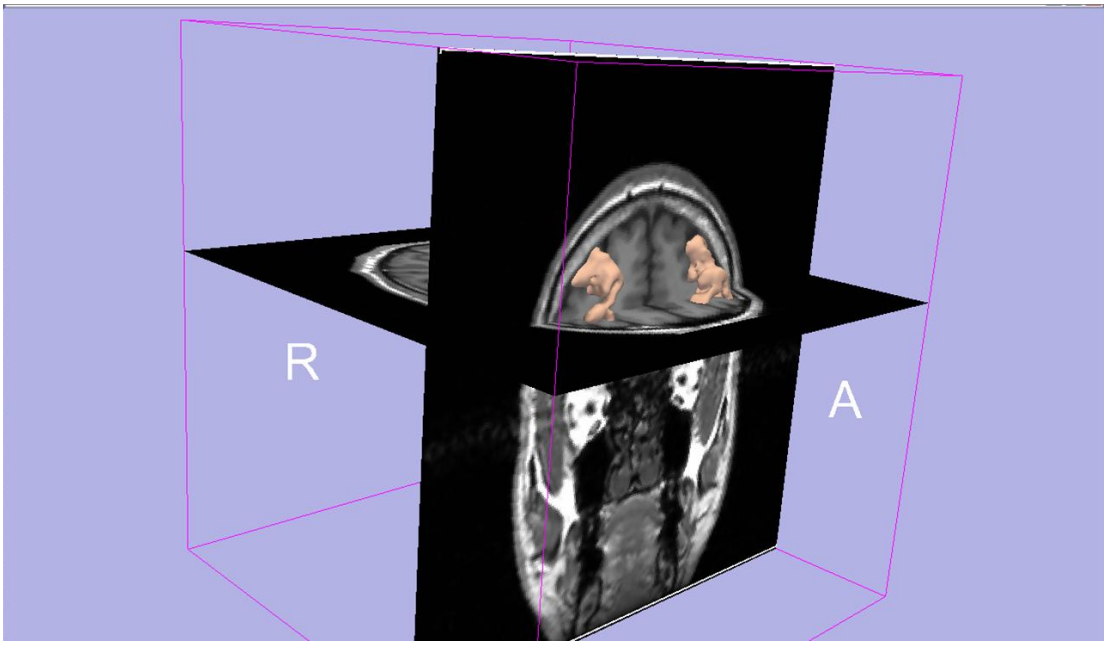

Figure 8. A model of the DLPFC created with the semi-automatic segmenter viewed in 3D-SLICER

Acknowledgements

This work is part of the National Alliance for Medical Image Computing (NAMIC), funded by the National Institutes of Health through the NIH Roadmap for Medical Research, Grant U54 EB005149. Information on the National Centers for Biomedical Computing can be obtained from http://nihroadmap.nih.gov/bioinformatics.

REFERENCES

1. D. Weinberger, K. Berman, and R. Zec, "Physiologic dysfunction of dorsolateral prefrontal cortex in schizophrenia: 1 regional cerebral blood flow evidence," *Archives of General Psychiatry* **43**(2), pp. 114–124, 1986.

2. W. Perlstein, C. Carter, D. Noll, and J. Cohen, "Relation of prefrontal cortex dysfunction to working memory and symptoms in schizophrenia," *Am J Psychiatry* **158**, pp. 1105–1113, 2001.
3. L. T. van Elst, G. Valerius, M. Buchert, T. Thiel, N. Rusch, E. Bubl, J. Hennig, D. Ebert, and H. Olbrich, "Increased prefrontal and hippocampal glutamate concentration in schizophrenia evidence from a magnetic resonance spectroscopy study," *Biol Psychiatry* **in print**, 2005.
4. W. Kates, K. Antshel, R. Willhite, B. Bessette, N. AbdulSabur, and A. Higgins, "Gender-moderated dorsolateral prefrontal reductions in 22q11.2 deletion syndrome: Implications for risk for schizophrenia," *Child Neuropsychology* **11**(1), pp. 73–85, 2005.
5. G. Rajkowska and P. S. Goldman-Rakic, "Cytoarchitectonic definition of prefrontal areas in the normal human cortex: Ii. variability in locations of areas 9 and 46 and relationship to the talairach coordinate system," *Cerebral Cortex* **5**(4), pp. 323–337, 1995.
6. J. Melonakos and A. Tannenbaum, "Knowledge-based segmentation of brain mri scans," *In submission* , 2006.
7. P. Teo, G. Sapiro, and B. Wandell, "Creating connected representations of cortical gray matter for functional MRI visualization," *IEEE Trans. Med. Imag.* **16**(6), pp. 852–863, 1997.
8. S. Haker, G. Sapiro, and A. Tannenbaum, "Knowledge-based segmentation of sar data with learned priors," *IEEE TIP* **9**, pp. 298–302, 2000.
9. P. Teo, G. Sapiro, and B. Wandell, "Anisotropic smoothing of posterior probabilities," in *In Proc. ICIP, Santa Barbara, CA*, 1997.
10. A. Zijdenbos, B. Dawant, and R. Marjolin, "Morphometric analysis of white matter lesions in mr images: Methods and validation," *IEEE TMI* **13**(4), pp. 716–724, 1994.